International Journal of Applied Earth Observation and Geoinformation 144 (2025) 104909

Contents lists available at ScienceDirect

International Journal of Applied Earth Observation and Geoinformation

journal homepage: www.elsevier.com/locate/jag

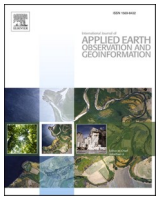

Combining two water type classification schemes for semi-analytical estimation of suspended particulate matter concentrations in various water bodies

Mailisu [a], Dalin Jiang [b], Bunkei Matsushita [c,*]

[a] Graduate School of Life and Environmental Science, University of Tsukuba, Tennoudai 1-1-1, Tsukuba 305-8578, Japan
[b] Earth and Planetary Observation Sciences (EPOS), Biological and Environmental Sciences, Faculty of Natural Sciences, University of Stirling, Stirling FK9 4LA, UK
[c] Faculty of Life and Environmental Sciences, University of Tsukuba, Tennoudai 1-1-1, Tsukuba 305-8572, Japan

ARTICLE INFO

Keywords:
Semi-analytical method
Optical water type classification
Particle composition classification
Suspended particulate matter

ABSTRACT

Retrieval of suspended particulate matter concentration (SPM) from remote-sensing reflectance (R_{rs}) is useful for frequent and widespread monitoring of water quality. However, R_{rs} values vary not only with SPM but also with particle composition (organic-dominated or mineral-dominated) and colored dissolved organic matter (CDOM), making it difficult to accurately estimate SPM in diverse aquatic environments using a single algorithm. In this study, two water type classification schemes: optical water type classification scheme and particle composition classification scheme, were integrated into a semi-analytical method to improve the accuracy of SPM estimation in various water bodies. By combining these two classification schemes, we classified water bodies around the world into 12 water types and developed an SPM estimation algorithm for each water type. Using 4,513 in situ R_{rs}-SPM measurements, the performance of the new SPM estimation algorithm was compared to that of 11 existing SPM estimation algorithms, and the results show that the median absolute percentage error (*MdAPE*) was reduced from 51.3 to 58.9% to 43.2%. The performance of the proposed method was also evaluated using 226 satellite matchups, with an *MdAPE* of 43.4%. Further comparative analysis and showcases based on several satellite images demonstrate that the two water type classification schemes play different roles that can effectively enhance the accuracy of SPM estimation.

1. Introduction

Suspended particulate matter (SPM) significantly contributes to biogeochemical cycling of materials in aquatic environments due to its widespread presence, mobility, and effects on water quality, ecosystem productivity, and carbon sequestration (Eisma, 1993; Beusen et al., 2005; Torregroza-Espinosa et al., 2020; Szeligowska et al., 2024). Therefore, knowing the distribution of SPM around the world is essential to understand earth system processes and address challenges related to water resources, ecosystems, and human health (Huynh et al., 2024; Liu et al., 2024).

The use of satellite remote sensing allows for efficient and regular observation of SPM in aquatic environments worldwide. The concentration of SPM represents the sum of the two optically active substances (OASs, i.e., phytoplankton and non-algal particles) and can be estimated from remote sensing reflectance (R_{rs}) or water-leaving reflectance (ρ_w) using estimation algorithms (e.g., Nechad et al., 2010; Siswanto et al., 2011; Novoa et al., 2017). In general, there are two types of SPM estimation algorithms: empirical and semi-analytical. The former (including machine learning approaches) is highly dependent on the training data used in algorithm development and therefore often has limited applicability. In contrast, the latter does not require frequent recalibration and has good applicability, as the empirical relationships it contains are only of secondary importance in SPM estimation (Jiang et al., 2021, 2023). Thus, semi-analytical algorithms can potentially become globally applicable algorithms.

However, empirical and semi-analytical algorithms both encounter two major issues when applied to water bodies with a wide range of SPM concentrations. First, R_{rs} saturate in waters with high SPM concentrations at shorter wavelengths (e.g., green and red bands), so R_{rs} at longer wavelengths (e.g., near-infrared bands) must be used to estimate SPM in such waters (Doxaran et al., 2009). To address this challenge, many

* Corresponding author.
E-mail address: matsushita.bunkei.gn@u.tsukuba.ac.jp (B. Matsushita).

https://doi.org/10.1016/j.jag.2025.104909
Received 14 July 2025; Received in revised form 1 October 2025; Accepted 12 October 2025
Available online 16 October 2025

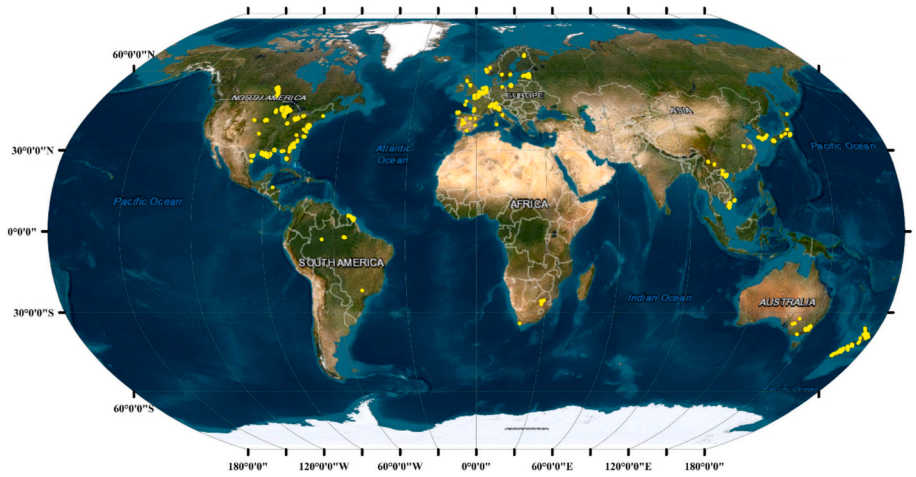

Fig. 1. Distribution map of water bodies (Yellow dots). The basemap source from Esri, Maxar, Earthstar Geographics, and the GIS User Community.

studies have developed multiple SPM estimation algorithms along with optical water type (OWT) classification schemes to accommodate different water bodies (Gernez et al., 2017; Jiang et al., 2021; Stramski et al., 2023). For example, Novoa et al. (2017) used an OWT-based water type classification scheme (i.e., based on the magnitude of R_{rs} at 665 nm) to classify water bodies into five OWTs and developed five corresponding algorithms to estimate SPM concentrations from low to high using the green, red, near-infrared (NIR) bands, or a combination of thereof, respectively. Second, due to differences in refractive indices between organic- and mineral-dominated waters (Aas, 1996) and the variations in particle size, shape, and density in natural environments (Babin et al., 2003; Shi & Wang, 2019), the R_{rs} of a water body is not determined solely by the OAS concentration in the water body. Teng et al. (2025) clearly show that the same SPM concentration corresponds to different R_{rs} in both spectral shape and magnitude. This challenge also makes it difficult to estimate OAS concentrations (e.g., SPM concentrations) using a single estimation algorithm. Therefore, Teng et al. (2025) established a water type classification scheme that relies on the particle composition (PC) of water bodies (hereafter referred to as the PC-based water type classification scheme), classified water bodies into three categories (organic-rich, mineral-rich, and extremely mineral-rich), and developed three PC-specific algorithms to estimate the SPM concentrations in each category. So far, it is unclear whether combining the two water type classification schemes can simultaneously address the two challenges mentioned above.

Recently, Jiang et al. (2021) proposed a semi-analytical algorithm to estimate SPM concentrations in different water bodies. They first proposed an OWT classification approach based on water turbidity, in which water bodies were divided into four types: clear, moderate turbidity, high turbidity, and extreme turbidity. Then, an appropriate reference wavelength (λ_0) was selected and the original quasi-analytical algorithm (QAA-v5, Lee et al., 2002) or its modified version (Yang et al., 2013; IOCCG, 2014) was applied to estimate the particulate backscattering coefficient ($b_{bp}(\lambda_0)$) for each water type. Finally, the obtained $b_{bp}(\lambda_0)$ values were converted to SPM concentrations for each water type using fixed mass-specific particulate backscattering coefficient ($b^*_{bp}(\lambda_0)$) values based on the assumption that the $b_{bp}(\lambda_0)$ values depend only on the SPM concentration. However, this assumption does not necessarily hold true, as natural waters typically exhibit a variety of particle compositions (Woźniak et al., 2010; Stramski et al., 2023). Therefore, it is believed that the particle composition of a water body can have a significant effect on the $b^*_{bp}(\lambda_0)$ value of the water body, and the PC-based water type classification scheme has the potential to help select more appropriate $b^*_{bp}(\lambda_0)$ values for water bodies with different particle compositions.

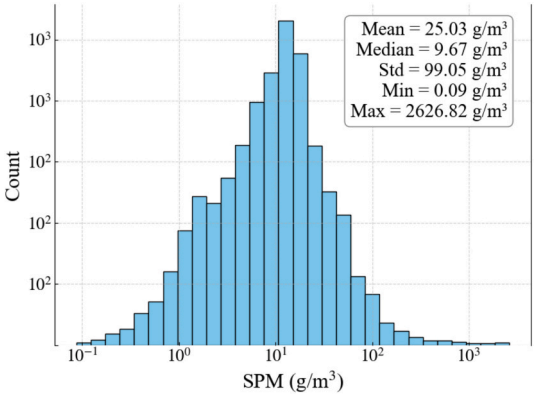

Fig. 2. Histogram of SPM concentration distribution for the final in situ dataset (N = 4,513).

Consequently, the primary goal of this study is to establish a semi-analytical algorithm capable of estimating SPM concentrations in devise water environments where both turbidity and particle composition vary. Specifically, we aim to: (1) propose a new water type classification algorithm that can account for changes in both turbidity and particle composition of a water body; (2) develop a series of sub-algorithms to estimate more accurate SPM concentrations for each water type defined in this study; (3) evaluate the performance of the new algorithm using a comprehensive in situ dataset and satellite matchups.

2. Data used

2.1. In-situ datasets

To evaluate the performance of the developed algorithm, a comprehensive in-situ dataset was collected from the Global Reflectance community dataset for Imaging and optical sensing of Aquatic environments (GLORIA, Lehmann et al., 2023). The GLORIA dataset contains 7,572 R_{rs} measurements, but only 4,621 R_{rs} spectra have corresponding SPM data. Of the 4,621 R_{rs} spectra, 108 R_{rs} spectra were removed due to missing required wavelengths or estimated negative b_{bp} values when using the Jiang et al. (2021) method. Consequently, a total of 4,513 R_{rs}-SPM observations were preserved for further analysis. Furthermore, the method developed by Jiang et al. (2020) were applied to remove residual reflective skylights from all remaining R_{rs} spectra. Finally, the R_{rs} spectra were transformed into the 13 MERIS (Medium Resolution Imaging Spectrometer) spectral bands (413, 443, 490, 510,

Table 1
Summary of the satellite matchups used to validate the SPM estimation algorithm developed in this study.

Matchup dataset	Site name(Number of matchups)	Image date(Number of scenes)	Sensor
GLORIA	English Channel (13)	2009/6/16–2010/07/06 (8)	MERIS
	Gulf of Tonkin (6)	2011/11/10–2011/11/15 (3)	
	Lake Kasumigaura (21)	2006/02/18–2010/05/18 (3)	
	Iznájar (4)	2007/07/04 (1)	
	Atlantic Ocean (1)	2009/06/01, 2010/06/13 (2)	
	Rosarito (2)	2007/07/13 (1)	
Jiang21	Akan (2)	2019/08/27 (1)	OLCI
	Green Bay (4)	2019/06/06, 2019/07/24 (2)	
	Poygan (5)	2018/08/23, 2018/09/11 (2)	
	Winnebago (6)	2016/09/20 (1)	
	Lac Vieux Desert (3)	2016/06/28 (1)	
	Winneconne (4)	2019/09/11 (1)	
	Lake Kasumigaura (85)	2004/07/07–2020/03/11 (16)	MERIS, OLCI
	Suwa (69)	2006/06/06–2020/06/17 (57)	
	Taihu (1)	2007/01/07 (1)	MERIS

560, 620, 665, 681, 709, 754, 761, 779, and 865 nm) using MERIS spectral response function.

Fig. 1 shows the distribution map of the water bodies from which the data used in this study were collected. The 4,513 R_{rs}-SPM data pairs were collected from 394 water bodies globally, including 146 in North America, 110 in Europe, 98 in Oceania, 21 in Asia, six in Africa, and four in South America. SPM values range from 0.09 g/m^3 to 2626.82 g/m^3, with half of them below 10 g/m^3 (median = 9.7 g/m^3, Fig. 2).

2.2. Satellite datasets

The developed algorithm was also evaluated using real satellite data. For this purpose, two matchup datasets were collected. The first dataset was compiled from the GLORIA dataset (Lehmann et al., 2023) and the corresponding MERIS Level 1B data (https://oceancolor.gsfc.nasa.gov/). The second dataset was obtained from Jiang et al. (2021) with MERIS and Sentinel-3 Ocean and Land Colour Instrument (OLCI) Level 1 data (https://merisfrs-merci-ds.eo.esa.int). Atmospheric correction was performed to all MERIS and OLCI Level 1 data to obtain R_{rs} by ourselves using the Case 2 Regional Coast Colour (C2RCC) processor (Brockmann et al., 2016) in SNAP version 9.0.0.

To collect valid matchups, we applied the following criteria to the two datasets: (1) no contamination by clouds or cloud shadows; (2) the time between satellite image acquisition and in-situ measurement is within ± 3 h; (3) there are five or more valid pixels within a 3 × 3 box, and the coefficient of variation (CV) of these valid pixels does not exceed 0.3 (Bailey and Werdell, 2006; Harding et al., 2005).

Finally, the first dataset contains 47 matchups, and the second dataset contains 179 matchups taken from 10 lakes between 2004 and 2020. Overall, a total of 226 matchups were used to evaluate the developed algorithm (see Table 1 for details).

3. 3.Methods

3.1. Development of a semi-analytical algorithm for estimating SPM in various aquatic environments

For any water body, SPM can be analytically calculated by the following formula:

$$SPM = b_{bp}(\lambda_0)/b^*_{bp}(\lambda_0) \quad (1)$$

where $b_{bp}(\lambda_0)$ and $b^*_{bp}(\lambda_0)$ are the particulate backscattering coefficient and the mass-specific particulate backscattering coefficient, respectively. λ_0 is the reference wavelength selected according to the OWT-based classification approach (Jiang et al., 2021, also see Section 3.1.1).

3.1.1. Semi-analytical estimation of $b_{bp}(\lambda_0)$ based on optical water type (OWT) classification

The OWT-based water type classification method proposed by Jiang et al. (2021) was adopted in this study to enable semi-analytically estimation of $b_{bp}(\lambda_0)$ across diverse water bodies. This method consists of three main steps (Table 2). In step 1, the world's waters are classified into four OWTs according to their turbidity levels. This OWT classification scheme is used to determine the most appropriate reference wavelength (λ_0) that meets the fundamental requirements of the QAA corresponding to each OWT. Specifically, QAA-v5 (Lee et al., 2002, λ_0 = 560) is used for clear waters, QAA-v6 (IOCCG, 2014, λ_0 = 665) for moderately turbid waters, QAA-Turbid (Yang et al., 2013, λ_0 = 754) for highly turbid waters, and QAA-Turbid (Jiang et al., 2021, λ_0 = 865) is used for extremely turbid waters.

In step 2, the corresponding empirical equations are used to estimate the non-water absorption coefficient ($a_{nw}(\lambda_0)$) and then the total absorption coefficient ($a(\lambda_0)$). Finally, in step 3, the $b_{bp}(\lambda_0)$ for each OWT can be obtained.

3.1.2. Selection of appropriate $b^*_{bp}(\lambda_0)$ based on particle composition (PC) classification

Unlike $b_{bp}(\lambda_0)$, there is no effective method yet to estimate $b^*_{bp}(\lambda_0)$

Table 2
An OWT-based algorithm for estimating $b_{bp}(\lambda_0)$ across diverse water bodies (Jiang et al., 2021).

Step0	$r_{rs}(\lambda_0) = R_{rs}(\lambda_0)/(0.52 + 1.7R_{rs}(\lambda_0))$ $u(\lambda_0) = \frac{-g_0 + \sqrt{(g_0)^2 + 4g_1 * r_{rs}(\lambda_0)}}{2g_1}$, *where* $g_0 = 0.089$ *and* $g_1 = 0.1245$			
Step1	Optical water type classification Clear water (λ_0 = 560nm,, QAA-v5)	Moderately turbid water (λ_0 = 665nm, QAA-v6)	Highly turbid water (λ_0 = 754nm, QAA-Turbid)	Extremely turbid water (λ_0 = 865nm, QAA-Turbid)
Step2	$a_{nw}(560) = 10^{-1.146-1.366X-0.469X^2}$ $X = log(\frac{r_{rs}(443)+r_{rs}(490)}{r_{rs}(\lambda_0)+5\frac{r_{rs}(665)}{r_{rs}(490)}r_{rs}(665)})$	$a_{nw}(665) = 0.39(\frac{R_{rs}(\lambda_0)}{R_{rs}(443)+R_{rs}(490)})^{1.14}$	$a_{nw}(754) = 0$	$a_{nw}(865) = 0$
Step3	$a(\lambda_0) = a_{nw}(\lambda_0) + a_w(\lambda_0)$ $b_{bp}(\lambda_0) = \frac{u(\lambda_0)\times a(\lambda_0)}{1-u(\lambda_0)} - b_{bw}(\lambda_0)$			

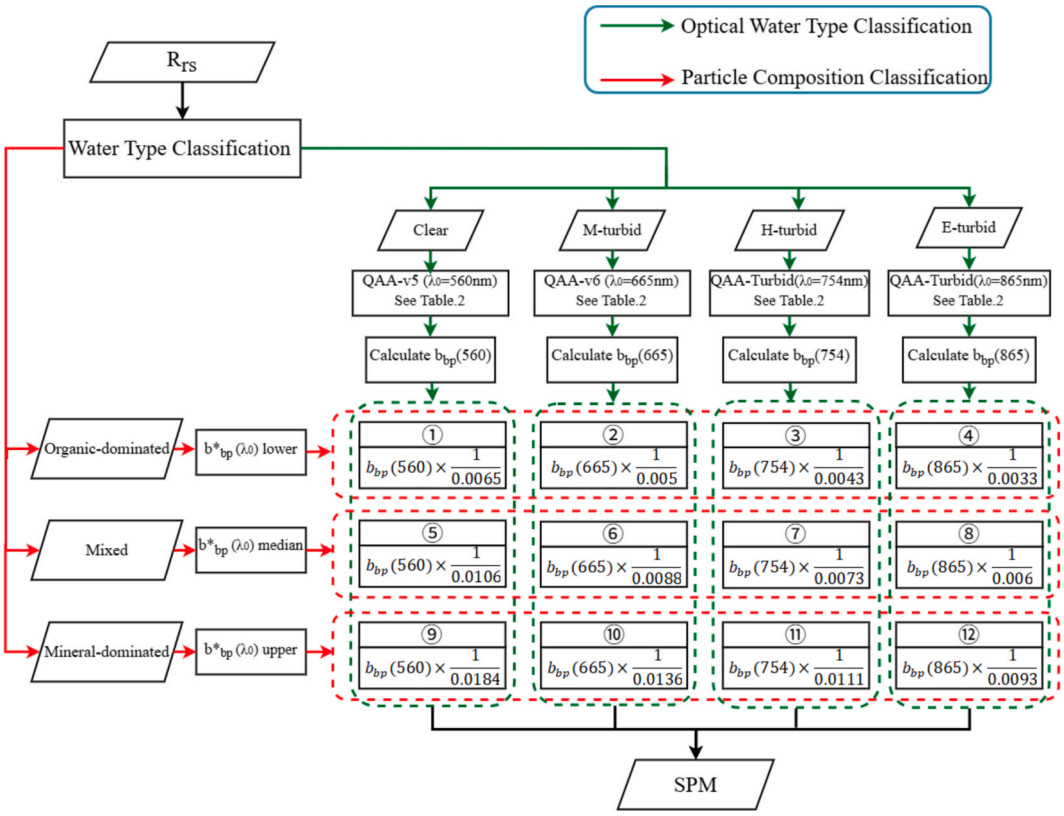

Fig. 3. Flowchart illustrates the SPM estimation algorithm developed in this study. The OWT-based water type classification scheme is used to identify the appropriate λ_0 and estimate $b_{bp}(\lambda_0)$ using the corresponding QAA. The particle composition classification scheme is used to select the appropriate $b^*_{bp}(\lambda_0)$.

from R_{rs}. On the other hand, previous studies have reported that the value of b^*_{bp} is strongly correlated with particle composition (Babin et al., 2003; Woźniak et al., 2010). For example, organic-dominated waters generally have low mass-specific particulate scattering coefficient (b^*_p) values, mineral-dominated waters have high values, and mixed waters have intermediate b^*_p values (Woźniak et al., 2010, b^*_{bp} is usually proportional to b^*_p). Therefore, the use of dynamic $b^*_{bp}(\lambda_0)$ values instead of fixed $b^*_{bp}(\lambda_0)$ values may improve the accuracy of SPM estimation in global waters. Specifically, in this study, we propose to apply the lower quartile, median, and upper quartile values of $b^*_{bp}(\lambda_0)$ presented in Jiang et al. (2021) to organic-dominated, mixed, and mineral-dominated waters, respectively (the values are shown in Fig. 3 and the associated descriptions are given in Supplementary Table S2).

The ratio of particulate organic carbon (POC) to SPM (POC/SPM), which can be empirically estimated from R_{rs}, has been used to identify the particle composition of water bodies. For example, Stramski et al. (2023) proposed an empirical equation to estimate the POC/SPM ratio from R_{rs} based on data collected from the western Arctic Ocean. This equation was recently modified by Teng et al. (2025) using data collected from a larger number of water bodies. Therefore, in this study, the updated formula recommended by Teng et al. (2025) was adopted to estimate the POC/SPM ratio:

$$\frac{POC}{SPM} = 10^{(-0.973R_G - 3.323)} \quad (2)$$

$$R_G = \log(R_{rs}(560))$$

Meanwhile, Woźniak et al. (2010) proposed two thresholds of POC/SPM ratio (0.06 and 0.25) to classify water bodies into organic-dominated (POC/SPM $\geq$ 0.25), mixed (0.06 $<$ POC/SPM $<$ 0.25), and mineral-dominated (POC/SPM $\leq$ 0.06) waters. These two thresholds were subsequently modified by Stramski et al. (2023) (i.e., 0.12 and 0.28) to divide the Arctic Ocean into three similar categories. Recently, Teng et al. (2025) pointed out that the organic-dominated and mixed categories of Stramski et al. (2023) showed similar mean R_{rs} spectral shapes and should be merged into the same organic-rich category (POC/SPM $\geq$ 0.12). Consequently, in this study, we propose a new particle composition (PC) classification scheme by combining the thresholds recommended in the above three studies. That is, POC/SPM $\geq$ 0.12 for organic-dominated waters, 0.06 $<$ POC/SPM $<$ 0.12 for mixed waters, and POC/SPM $\leq$ 0.06 for mineral-dominated waters.

3.1.3. *Specific SPM estimation algorithm based on two water type classification schemes*

Using the above two water type classification schemes (OWT and PC), water bodies around the world can be classified into 12 water types: (1) organic-dominated and clear waters (O-Clear), (2) organic-dominated and moderately turbid waters (O-M-turbid), (3) organic-dominated and highly turbid waters (O–H-turbid), (4) organic-dominated and extremely turbid waters (O-E-turbid), (5) mixed and clear waters (M-Clear), (6) mixed and moderately turbid waters (M-M-turbid), (7) mixed and highly turbid waters (M-H-turbid), (8) mixed and extremely turbid waters (M-E-turbid), (9) mineral-dominated and clear waters (Mi-Clear), (10) mineral-dominated and moderately turbid waters (Mi-M-turbid), (11) mineral-dominated and highly turbid waters (Mi-H-turbid), and (12) mineral-dominated and extremely turbid waters (Mi-E-turbid). Accordingly, we developed 12 water type specific SPM estimation algorithms (Fig. 3). For example, if a water pixel is classified as O–H-turbid water type, the third SPM estimation formula in Fig. 3 is selected (intersection of the red and green boxes in Fig. 3).

3.2. *Accuracy assessment*

To evaluate the agreement between estimated SPM(y'_i) and measured

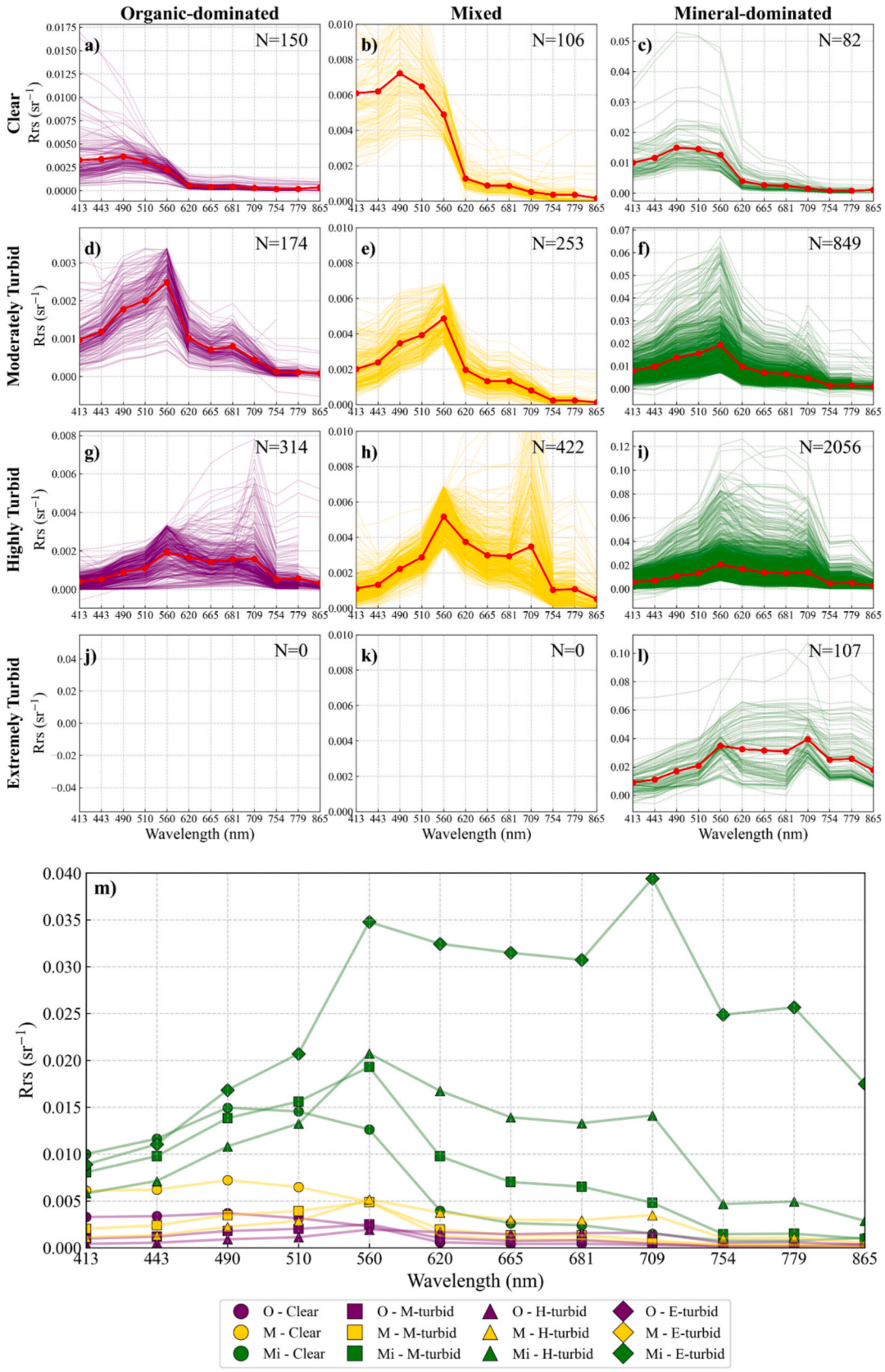

Fig. 4. R_{rs} spectra of the 12 water types identified in this study. Rows indicate different optical water types, and the columns represent each particle composition type. a)–l) show the individual R_{rs} spectra (light lines), the mean R_{rs} spectrum (red line). m) summarizes the mean R_{rs} spectra across all types. See Section 3.1.3 for abbreviations for each water type.

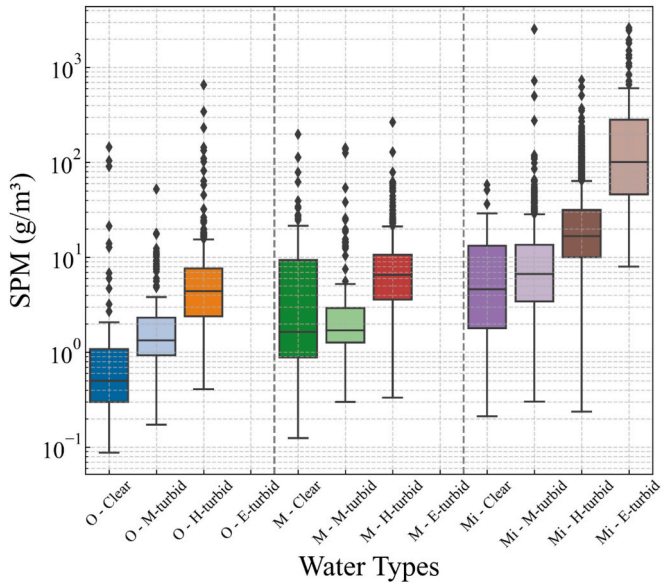

Fig. 5. Boxplots of SPM distribution for the 10 detected water types. See Section 3.1.3 for abbreviations for each water type. Note: no data for O-E-turbid and M−E−turbid waters.

values SPM(y_i), three widely used metrics were employed: the root mean square error (*RMSE*), median absolute percentage error (*MdAPE*), and *Bias*. These metrics are calculated as follows:

$$RMSE = \sqrt{\frac{1}{N}\sum_{i=1}^{N}\left(\log(y_i') - \log(y_i)\right)^2} \quad (3)$$

$$MdAPE = median\left|\frac{y_i' - y_i}{y_i}\right| \times 100\% \quad (4)$$

$$Bias = \frac{1}{N}\sum_{i=1}^{N}\left(\log(y_i') - \log(y_i)\right) \quad (5)$$

where N is the total amount of data. Additionally, the coefficient of determination (R^2) and *Slope* are also calculated after logarithmic transformation. Model II regression was applied to estimate the fitted line and slope.

4. Results

4.1. Water type classification

Fig. 4 shows the classification results based on the two water type classification schemes (OWT and PC). Of the 12 defined water types, 10 were found in the GRORIA R_{rs} (N = 4,513) dataset used in this study, except for O-E-turbid and M-E-turbid waters. Of 10 detected water types, Mi-H-turbid waters account for the largest proportion (46 %, N = 2,056), followed by Mi-M-turbid waters (19 %, N = 849), M-H-turbid waters (9 %, N = 422), O–H-turbid waters (7 %, N = 314), M-M-turbid waters (6 %, N = 253), O-M-turbid waters (4 %, N = 174), O-Clear waters (3 %, N = 150), Mi-E-turbid waters (2 %, N = 107), M-Clear waters (2 %, N = 106), and Mi-Clear waters (2 %, N = 82). From the figure, we can see that R_{rs} belonging to the same OWT may have different particle compositions (see figures in the same row) and that R_{rs} with similar particle compositions may be classified into different OWTs (see figures in the same column). In general, the R_{rs} spectral shape varies depending on the OWT classification, whereas the magnitude of R_{rs} strongly depends on the PC classification (mineral-dominated > mixed > organic-dominated, Fig. 4m).

Fig. 5 shows the statistical results of SPM distribution for each water type. It shows that several water types with different OWT as well as different PC can have similar SPM values. This result indicates that it is difficult to select the optimal SPM estimation algorithm based on only one water type classification scheme (OWT or PC). In other words, combining the two water type classification schemes could improve the accuracy of SPM estimation.

4.2. Performance evaluation of the newly developed semi-analytical algorithm using in situ data

Fig. 6 shows a comparison of the estimated SPM concentrations using different algorithms with the in situ measured SPM concentrations (N = 4,513). These algorithms include three empirical algorithms that use only a single equation (Nechad et al., 2010; Siswanto et al., 2011; Woźniak et al., 2016; hereafter referred to as Nechad10, Siswanto11, and Woźniak16, respectively), five empirical algorithms using multiple equations based on different OWT classification (Han et al, 2016; Gernez et al., 2017; Novoa et al., 2017; Stramski et al., 2023; hereafter referred to as Han16, Han16-NIR, Gernez17, Novoa17, and Stramski23, respectively), one algorithm that combines semi-analytical, machine learning and empirical approaches (Balasubramanian et al., 2020; hereafter referred to as SOLID or Bala20), one empirical algorithm using multiple equations based on PC classification (Teng et al., 2025; hereafter referred to as Teng25), one semi-analytical algorithm using multiple equations based on OWT classification (Jiang et al., 2021; hereafter referred to as Jiang21), and the new semi-analytical algorithm developed in this study (Supplementary Table S1).

It is not surprising that empirical algorithms using a single equation have difficulty dealing with SPM estimation over a wide range (Figs. 6a–6c). Nechad10 shows a large overestimation at low SPM concentrations, while Woźniak16 shows a large underestimation at high SPM concentrations. Siswanto11 also has lower estimation accuracy at both low and high SPM concentrations. This issue can be mitigated by switching between multiple equations based on water type classification (Fig. 6e, Figs. 6g–6j). For example, compared with Nechad10 (Fig. 6a), Han16-NIR (Fig. 6i) significantly improved the SPM estimation accuracy at both low and high SPM concentrations by selecting a more appropriate equation for each OWT (Type I: $R_{rs}(665) \leq 0.03$; Type II: $R_{rs}(665) \geq 0.04$; Type III: $0.03 < R_{rs}(665) < 0.04$). With the help of PC classification, Teng25 also shows no obvious over or underestimation across the entire SPM range (Fig. 6j).

However, the typical limitation of empirical algorithms, namely that their performance is highly dependent on the calibration data used, remains unresolved even when the multiple equations are applied. Gernez17 and Novoa17 used similar OWT classification method but were calibrated using different datasets and therefore performed differently on the GLORIA dataset, especially for data with high SPM concentrations (Figs. 6d and 6e). This limitation can be mitigated by using semi-analytical methods instead of empirical methods. From Figs. 6k and 6l, it can be seen that the two semi-analytical algorithms show better applicability across the entire dataset compared to all the empirical algorithms. In particular, the newly developed algorithm in this study showed the best performance in SPM estimation, with the smallest MdAPE (43.2 % vs. 51.3 %–58.9 %) and the second smallest RMSE (0.45 vs. 0.44–0.57). Moreover, the slope is closest to 1 and the R^2 is the second highest (0.54 vs. 0.37–0.56), which indicates that the new algorithm can better capture the real SPM variation compared to other existing algorithms. However, given the Bias of 0.84, the new algorithm appears to slightly underestimate SPM.

To investigate how water type classification can aid in SPM estimation, we further compared the performance of three SPM estimation algorithms (Teng25, Jiang21 and this study) that use different water type classification methods for each water type defined in this study (Fig. 7, Table 3). By using the PC classification method proposed in this study (Section 3.1.2), the GLORIA dataset (N = 4,513) was classified into organic-dominated (N = 638, Figs. 7a–7c), mixed (N = 781, Figs. 7d–7f), and mineral-dominated (N = 3,094, Figs. 7g–7i) waters.

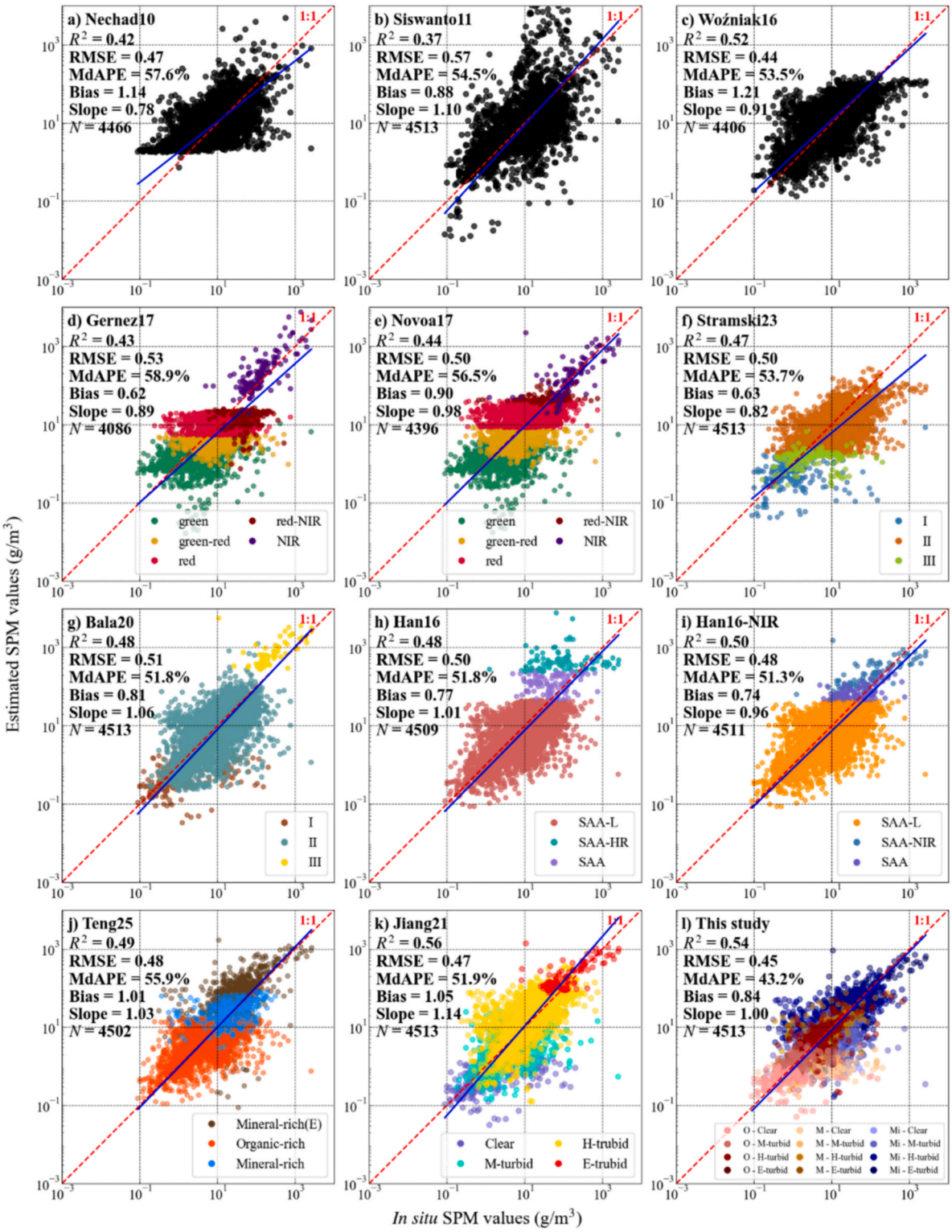

Fig. 6. Comparison of SPM concentrations estimated from in-situ measured R_{rs} using different algorithms with the in-situ measured SPM concentrations. The red and blue lines in each subfigure represent the 1:1 line and the fit line, respectively. The color of the dots in each subfigure represents the water type classification results for each SPM estimation algorithm.

The data for each PC water type were further classified into four types using the OWT-based classification approach in this study (see colors in Fig. 7). Because Teng25 used different POC/SPM thresholds and categories for PC classification, its classification results were represented using different marks (Figs. 7a, 7d, and 7g).

For the organic-dominated waters, Teng25 shows a significant underestimation (Bias = 0.57, slope = 0.60, Fig. 7a), which is significantly improved by the present study (Bias = 0.88 and slope = 0.94, Fig. 7c). Additionally, the MdAPE and RMSE also decreased from 49.9 % to 44.5 % and from 0.52 to 0.43, respectively. All 638 organic-dominated water samples were classified as "organic-rich" water by Teng25, so the SPM concentrations estimated by Teng25 are based on a single algorithm

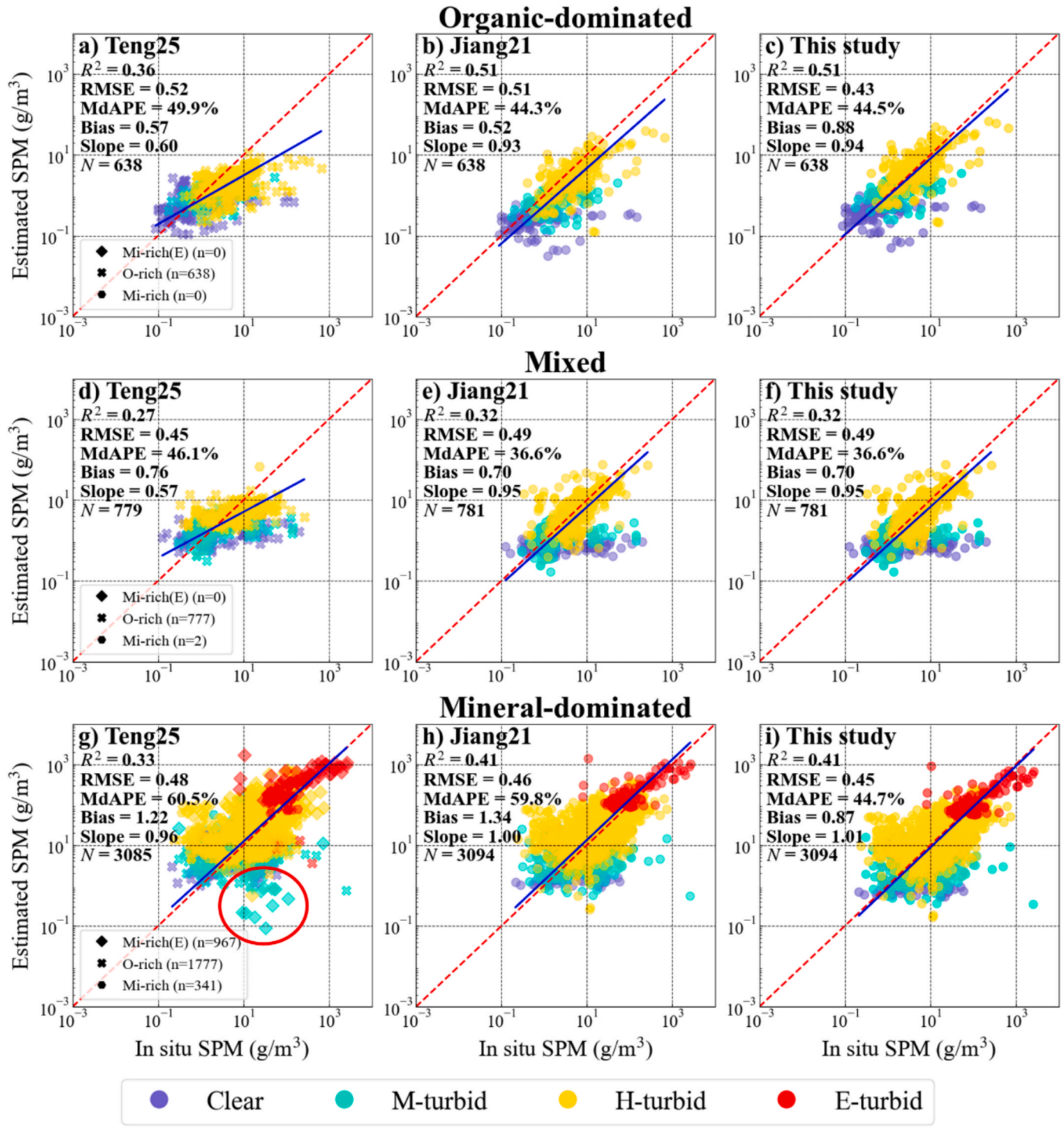

Fig. 7. Comparison of estimated SPM concentrations with different algorithms (Teng25, Jiang21 and this study) and in-situ measured SPM concentrations for different water types. The first row shows organic-dominated water samples, the second row shows mixed water samples, and the third row shows mineral-dominated water samples. The colors of the dots represent the OWTs defined in Jiang et al. (2021). The marks in the first column represent PC-based water types as defined in Teng et al. (2025). The red line represents the 1:1 line, and the blue line represents the fit line in each subfigure.

using R_{rs} at a single band of 665 nm (Teng et al., 2025). In contrast, these organic-dominated water samples were further classified into clear (N = 150, purple dots), moderately turbid (N = 174, blue dots), and highly turbid water (N = 314, yellow dots) using OWT classification method, and different algorithms (both the bands and the equations used) were used to estimate SPM in each sub-water type. Compared with the performance of Jiang21 (Fig. 7b, use median $b^*_{bp}(\lambda_0)$ without PC classification), although the MdAPE is slightly larger (44.3 % vs. 44.5 %), our method (use the lower quartile $b^*_{bp}(\lambda_0)$ based on the PC classification) reduces the RMSE (from 0.51 to 0.43) and improves the Bias significantly (from 0.52 to 0.88), indicating that the PC classification allows us to select a more appropriate $b^*_{bp}(\lambda_0)$ value.

For mixed waters, our method also improved SPM estimates compared to Teng25, reducing the MdAPE from 46.1 % to 36.6 %. Similarly, this improvement comes from further use of OWT

Table 3
Performance evaluation metrics of the three algorithms (Teng25, Jiang21, this study) for each water type defined in this study. See Section 3.1.3 for abbreviations for each water type. Values with orange background represent the lowest values for MdAPE and RMSE, the values closest 1 for Bias, R^2, and slope.

Water type	Method	MdAPE	RMSE	Bias	R^2	Slope	N
O-Clear	Teng25	51.42	0.55	0.85	0.03	0.52	150
	Jiang21	48.93	0.67	0.41	0.02	0.44	150
	This Study	48.22	0.57	0.67	0.02	0.44	150
O-M-turbid	Teng25	42.25	0.41	0.67	0.12	0.51	174
	Jiang21	48.64	0.5	0.46	0.13	0.57	174
	This Study	42.58	0.38	0.81	0.13	0.57	174
O-H-turbid	Teng25	54.91	0.57	0.43	0.15	0.62	314
	Jiang21	40.31	0.42	0.62	0.4	0.87	314
	This Study	43.45	0.37	1.06	0.4	0.87	314
O-E-turbid	Teng25	–	–	–	–	–	–
	Jiang21	–	–	–	–	–	–
	This Study	–	–	–	–	–	–
M−Clear	Teng25	72.83	0.7	0.51	0.14	0.3	104
	Jiang21	72.04	0.87	0.27	0.05	0.17	106
	This Study	72.04	0.87	0.27	0.05	0.17	106
M-M-turbid	Teng25	46.35	0.42	0.94	0.06	0.48	253
	Jiang21	39.45	0.47	0.65	0.06	0.53	253
	This Study	39.45	0.47	0.65	0.06	0.53	253
M-H-turbid	Teng25	40.13	0.39	0.74	0.19	0.44	422
	Jiang21	29.85	0.34	0.94	0.39	0.94	422
	This Study	29.85	0.34	0.94	0.39	0.94	422
M-E-turbid	Teng25	–	–	–	–	–	–
	Jiang21	–	–	–	–	–	–
	This Study	–	–	–	–	–	–
Mi-Clear	Teng25	67.44	0.58	0.77	0.02	0.51	82
	Jiang21	66.08	0.69	0.41	0	−0.41	82
	This Study	75.64	0.85	0.24	0	−0.41	82
Mi-M−turbid	Teng25	72.24	0.52	1.16	0.03	0.77	842
	Jiang21	47.02	0.45	0.93	0.14	0.75	849
	This Study	45.45	0.5	0.6	0.14	0.75	849
Mi-H-turbid	Teng25	55.08	0.46	1.25	0.24	0.96	2054
	Jiang21	64.37	0.45	1.62	0.29	0.84	2054
	This Study	42.68	0.4	1.06	0.29	0.84	2054
Mi-E-turbid	Teng25	82.54	0.58	1.57	0.25	1.04	107
	Jiang21	74.99	0.46	1.71	0.46	0.62	107
	This Study	47.11	0.4	1.1	0.46	0.62	107
All Types	Teng25	55.9	0.48	1.01	0.49	1.03	4502
	Jiang21	51.9	0.47	1.05	0.56	1.14	4513
	This Study	43.2	0.45	0.84	0.54	1	4513

classification. In this category, Teng25 used the same single algorithm for most water samples (777 of 779), because these water samples were also classified by Teng25 as "organic-rich" waters (Fig. 7d). In contrast, our method estimated SPM using three different algorithms (both bands and equations used) based on the OWT classification (Fig. 7f). Especially in the M-H-turbid waters, compared to Teng25, our method shows significant improvements for all metrics (MdAPE: 40.13 % vs. 29.85 %, RMSE: 0.39 vs. 0.34, Bias: 0.74 vs. 0.94, R^2: 0.19 vs. 0.39, slope: 0.44 vs. 0.94; see Table 3 and yellow dots in Figs. 7d and 7f). Note that in this category, Jiang21 and our method show the same performance, because our method also uses the same $b^*_{bp}(\lambda_0)$ values (median) as Jiang21 based on PC classification (Fig. 7e vs. Fig. 7f).

Similarly, for mineral-dominated waters defined in this study, our method outperformed both Teng25 and Jiang21, with the lowest MdAPE (44.7 % vs. 59.8–60.5 %) and RMSE (0.45 vs. 0.46–0.48) values, due to the combined advantages of two water type classification schemes (Figs. 7g–7i). For example, the water samples within the red circle in Fig. 7g were classified as extremely mineral-rich waters by Teng25 and R_{rs} at 810 nm was used to estimate SPM, whereas these water samples were classified as Mi-M-turbid waters by our method and R_{rs} at 665 nm and upper quartile $b^*_{bp}(\lambda_0)$ were used to estimate SPM, leading to improved estimation accuracy (Fig. 7i). Additionally, for each sub-water type in this category, except for Mi-Clear waters, our method shows the lowest MdAPE for the other three sub-water types compared to both Teng25 and Jiang21 (Table 3). Overall, the above results indicate that using two water type classification schemes in combination is more effective in estimating SPM across different water bodies than using only one water type classification method.

4.3. Validation using satellite matchups and several showcases

We further assessed the performance of the new SPM estimation algorithm with satellite matchup data (Fig. 8). Among the 226 matchups, nine water types (excluding O-E-turbid water, M-E-turbid water, and Mi-Clear water) were detected. Overall, the accuracy of SPM estimated using our method from real MERIS and OLCI data was similar to that estimated from in-situ R_{rs}, with an MdAPE of 43.4 % and an RMSE of 0.39. Also, similar to the results obtained from the in-situ dataset, our method shows a slight underestimation of SPM, with a Bias value of 0.64. Moreover, the large slope value of 1.29 is mainly due to the apparent underestimation of SPM for several water samples within in-situ SPM below 10 g/m^3.

To additionally verify the capability of the newly proposed algorithm, we apply it to real satellite images and present the spatial distributions of OWT, PC, and SPM in four lakes (Fig. 9) and three estuaries (Fig. 10). From both figures, we can see that the spatial distribution pattern of the PC classification map (third column) is different from that of the OWT classification map (second column). For example, from the perspective of particle composition, most of the water pixels in Lake Kasumigaura (Japan) and Lake Turkana (Kenya) belong to mineral-dominated waters (Fig. 9A3 and 9D3). However, in terms of water turbidities, the water pixels of Lake Kasumigaura were classified into two types (highly turbid water and extremely turbid water, Fig. 9A2), whereas the water pixels of Lake Turkana were classified into three types (moderately turbid water, highly turbid water, and extremely turbid water, Fig. 9D2). The OWT and PC classification maps of other two lakes (Lake Erie in North America and Lake Qinghai in China) also show different distribution patterns, indicating that the two water type classification schemes can provide different information to select a more appropriate SPM estimation algorithm accordingly.

It can be clearly observed that in all three river estuaries, the OWT continuously changes from highly turbid or extremely turbid water to moderately turbid water, and then to clear water from the estuary toward the open ocean (Fig. 10A2, 10B2, 10C2). In addition, the particle composition patterns are similar: (1) mineral-dominated waters are commonly found in river mouths, (2) organic-dominated waters in the open ocean, and (3) mixed-water regions exist as a transition zone between them (Fig. 10A3, 10B3, and 10C3).

Furthermore, Figs. 9 and 10 show that the distribution patterns of SPM in the four example lakes and the three example estuaries are generally similar to the distribution patterns of the OWT classification, but not to the distribution patterns of the PC classification. This finding indicates that the SPM concentration in a water body is not directly related to the particle composition but has a strong influence on its optical properties.

5. Discussion

5.1. The need to combine the two water type classification schemes

In this study, a new semi-analytical algorithm was developed to estimate SPM from R_{rs} in various water bodies (Fig. 3). Our main contribution is the proposal to combine two water type classification schemes: (1) an OWT-based water type classification scheme adopted from Jiang et al. (2021), and (2) a PC-based water type classification scheme modified from Teng et al. (2025). The OWT-based water classification scheme allows categorizing water bodies into four types (clear, moderately turbid, highly turbid, and extremely turbid) based on the turbidity of the water body. Meanwhile, the PC-based water type classification scheme can classify water bodies into three types (organic-dominated, mixed, and mineral-dominated) based on the proportion of particulate

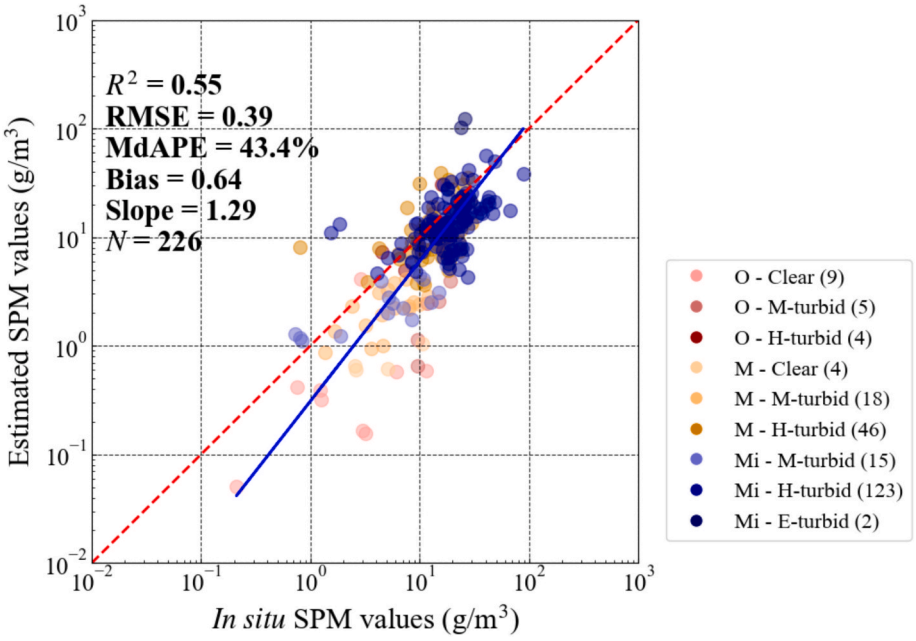

Fig. 8. Comparison of SPM concentrations estimated from satellite data using the newly developed SPM estimation algorithm with the in-situ measured SPM concentrations. The colors represent the water types defined in this study. The red and blue lines represent the 1:1 line and the fit line, respectively. The numbers in parentheses in the legend represent the amount of data for each type.

organic matter and minerals contained in the water body. Therefore, because water bodies classified into each OWT may have different particle compositions and water bodies classified into each PC type may also have different turbidities, a total of 12 water types can be classified by combining the two water type classification schemes. This finding is confirmed in Fig. 4, which shows that 10 water types were detected in the GLORIA dataset.

The results in Fig. 6 clearly show that the new algorithm can estimate more accurate SPM in different aquatic environments compared with other existing SPM estimation algorithms. To the best of our knowledge, all existing algorithms rely on one water type classification scheme (OWT-based or PC-based) and, due to limitations in available data, can only classify three to five water types to develop SPM estimation algorithms specific to each water type (Han et al., 2016; Balasubramanian et al., 2020; Stramski et al., 2023). Using only the OWT-based water type classification scheme can help select appropriate wavelengths for SPM estimation, but it cannot address the issue that water bodies with the same SPM concentration have different R_{rs} due to differences in particle composition (Teng et al., 2025, also see Figs. 4 and 5). On the other hand, using only the PC-based water type classification scheme makes it difficult to select appropriate wavelengths for more accurate SPM estimation (first and third columns in Fig. 7). In contrast, the new algorithm combines two different water type classification schemes to define 12 water types and allows different calculation formulas for each defined water type, thus improving the accuracy of SPM estimation across different water bodies (Table 3).

Certainly, not all of the existing algorithms compared in this study (Fig. 6) were developed for global SPM estimation across different water types. The aim of this comparison is to highlight the strengths and limitations of each algorithm using a global dataset (GLORIA) and the advances made in the SPM estimation algorithm developed in this study.

5.2. *Rationale for choosing appropriate $b^*_{bp}(\lambda_0)$ values based on particle composition classification*

In this study, the lower quartile, median, and upper quartile $b^*_{bp}(\lambda_0)$ values obtained from Jiang et al. (2021) were proposed to be used for organic-dominated, mixed, and mineral-dominated waters, respectively (Supplementary Table S2). Therefore, the $b^*_{bp}(\lambda_0)$ values used for organic-dominated and mineral-dominated waters in this study are smaller and larger, respectively, than those used in Jiang et al. (2021), who used fixed $b^*_{bp}(\lambda_0)$ values to estimate SPM in each OWT without considering differences in particle composition of water bodies. The fact that Jiang21′s underestimation of SPM in organic-dominated waters (Fig. 7b, Bias = 0.52) and overestimation of SPM in mineral-dominated waters (Fig. 7h, Bias = 1.34) were significantly improved in the present study (Fig. 7c, Bias = 0.88; Fig. 7i, Bias = 0.87) strongly supports the validity of our proposal.

Furthermore, our proposal is also supported by results reported in previous studies. Reynolds et al. (2016) reported that the b^*_{bp} values of mineral-dominated waters are two to three times higher than the b^*_{bp} values of organic-dominated waters; Neukermans et al. (2012) reported values of b^*_{bp} at 660 nm to be approximately 0.005 m^2 g^{-1} for organic particles and 0.012 m^2 g^{-1} for mineral particles; and Woźniak et al. (2016) observed a mean b^*_{bp} value at 560 nm in the Baltic Sea of 0.0073 m^2 g^{-1} with a CV of 29 %. These b^*_{bp} values are similar to those used in this study (e.g., 0.0065 m^2 g^{-1} for organic-dominated water and 0.0184 m^2 g^{-1} for mineral-dominated waters at 560 nm, and 0.005 m^2 g^{-1} for organic-dominated water and 0.0136 m^2 g^{-1} for mineral-dominated water at 665 nm).

In addition, in this study, the PC-based water type classification scheme is only used for selecting $b^*_{bp}(\lambda_0)$ values. This is because both the particle composition of the water body and the $b^*_{bp}(\lambda_0)$ values are independent of the SPM variations. In contrast, the $b_{bp}(\lambda_0)$ value has a direct relationship with R_{rs} (bio-optical model) and can therefore be altered not only by particle composition but also by SPM in the water body. Nevertheless, the $b_{bp}(\lambda_0)$ estimation based on the OWT-based water type classification and the corresponding QAA can help to identify the most appropriate wavelengths for selecting the $b^*_{bp}(\lambda_0)$ values. A total of 12 $b^*_{bp}(\lambda_0)$ values were identified in this study (Fig. 3).

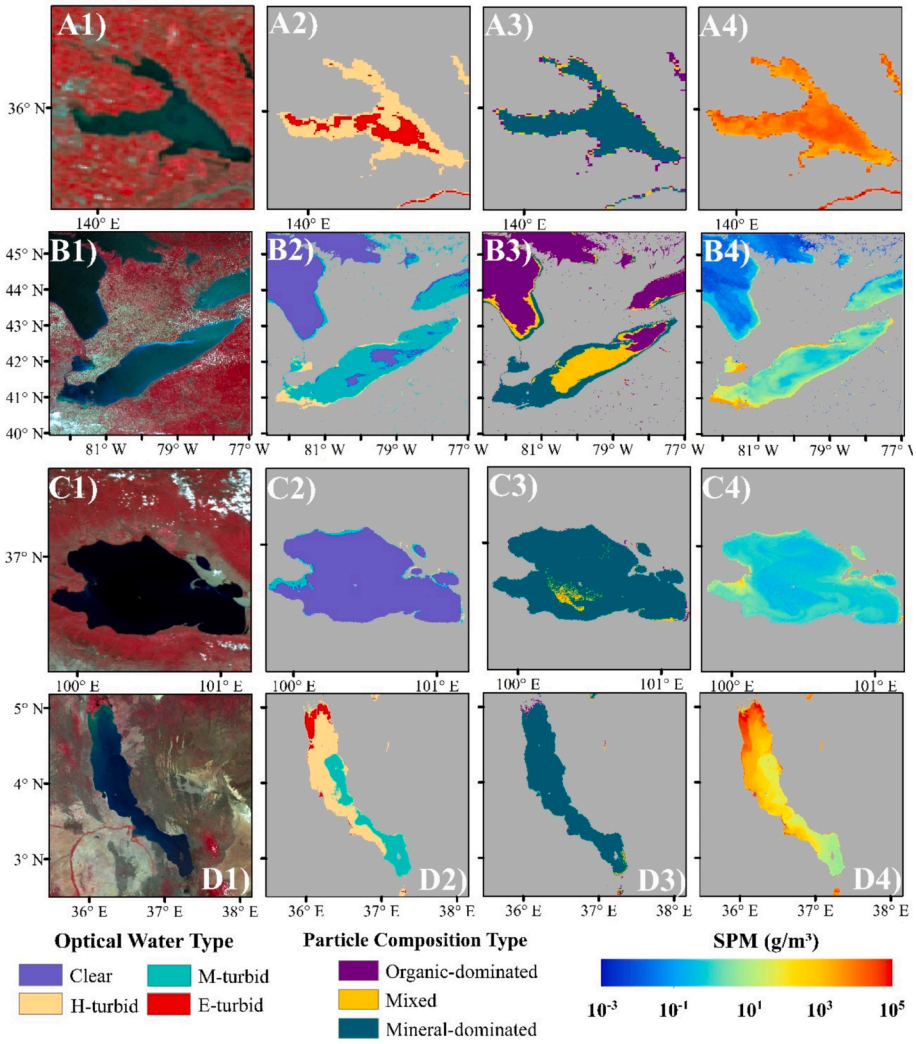

Fig. 9. Showcase maps for the four lakes. The first column displays the RGB OLCI (R: G: B = 17:8:6) or MERIS (R: G: B = 13:7:5) images, the second column shows the OWT classification maps, the third column shows the PC classification maps, and the fourth column shows the estimated SPM distribution maps. A1)-A4) Lake Kasumigaura, Japan (OLCI: Oct. 13, 2019); B1)-B4) Lake Erie, North America (MERIS: Jun. 02, 2011); C1)-C4) Lake Qinghai, China (OLCI: Jun. 29, 2020), D1)-D4) Lake Turkana, Kenya (OLCI: Mar. 13, 2020).

5.3. Applicability of the newly developed method and future challenges

In this study, $b_{bp}(\lambda_0)$ and the $b^*_{bp}(\lambda_0)$ are two intermediate variables for estimating SPM (Eq.1). To obtain $b_{bp}(\lambda_0)$ values, OWT-based water type classification was used to help select the appropriate reference wavelengths and QAAs for each OWT. This process allows for semi-analytical estimation of the $b_{bp}(\lambda_0)$ values by using different reference wavelengths for different OWTs to mitigate the absorption effects of non-water OASs (CDOM, NAP, phytoplankton) at the selected reference wavelength (Jiang et al., 2021). Meanwhile, the $b^*_{bp}(\lambda_0)$ values were selected from the synthetic data based on a combination of two water type classification schemes. To implement the PC-based water type classification scheme, we estimated the POC/SPM ratio from the R_{rs} using an empirical formula (Eq. (2) and determined two threshold values for the POC/SPM ratio using results from previous studies (Woźniak, et al., 2010; Teng et al., 2025). However, these empirical relationships are only used to select appropriate $b^*_{bp}(\lambda_0)$ values and are not used directly in estimating SPM and therefore are considered to be of only secondary importance in estimating SPM. With this consideration, the newly developed SPM estimation algorithm is semi-analytical and applicable to various aquatic environments (e.g., lakes, estuaries, coastal shelves, open ocean) without the need for readjustment.

The method developed in this study has two challenges. First, since Equation (2) for estimating the POC/SPM ratio used in this study is based only on data collected from limited water bodies (Teng et al., 2025), the applicability of this equation needs to be further evaluated using more field data. Additionally, the POC/SPM thresholds also need to be further tested. Meanwhile, in future work, it would also be worthwhile to test other methods for classifying water types. For example, Wang et al. (2016; Wang et al. (2023)) proposed using back-scattering efficiency to classify particle composition. More importantly, a semi-analytical method that can continuously estimate the $b^*_{bp}(\lambda_0)$ value from $R_{rs}(\lambda_0)$ could further improve the accuracy of SPM estimation. Second, the proposed method can only be applied to satellite data that can provide sufficient required bands (e.g. 620 nm, 754 nm). This limitation makes it difficult to apply the developed method to some satellite sensors with only a few wide bands, such as Landsat data (Teng et al., 2025). Future research should explore whether this method can be extended to apply to other satellite data.

6. Conclusions

In this study, we developed a new semi-analytical algorithm that can

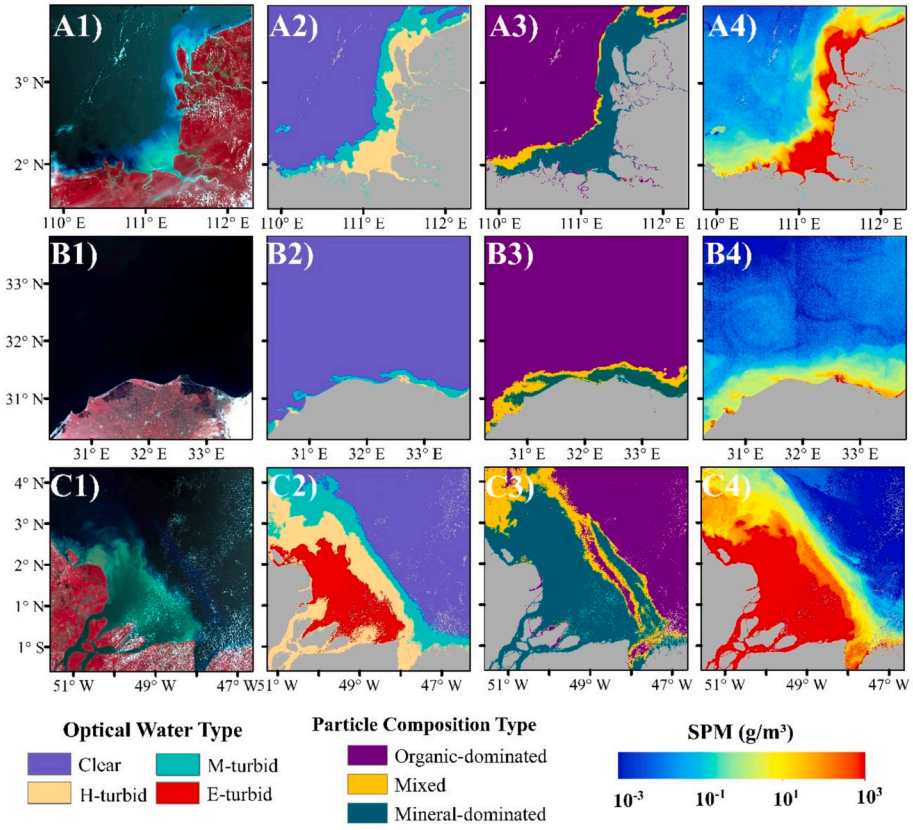

Fig. 10. Showcase maps for the three river estuaries. The first column displays the RGB OLCI (R: G: B = 17:8:6) or MERIS (R: G: B = 13:7:5) images, the second column shows the OWT classification maps, the third column shows the PC classification maps, and the fourth column shows the estimated SPM distribution maps. A1)-A4) Maludam River Estuary (MERIS: Apr. 25, 2009); B1)-B4) Nile River Estuary (OLCI: May 20, 2020); C1)-C4) Amazon River Estuary (OLCI: Aug. 24, 2019).

be applied to various aquatic environments for SPM estimation. The new algorithm creatively combines an OWT classification scheme that supports the selection of the optimal reference wavelength for semi-analytical retrieval of $b_{bp}(\lambda_0)$ from $R_{rs}(\lambda_0)$ and a particle composition classification scheme that helps determine the most appropriate $b^*_{bp}(\lambda_0)$ value for calculating SPM from $b_{bp}(\lambda_0)$. Through comparison with 11 existing SPM estimation algorithms using in situ data collected from water bodies around the world, validation exercises using satellite matchups from diverse aquatic environments, and application to actual satellite data from lakes and estuaries, we concluded that the new algorithm can provide more accurate SPM estimates overall than other existing algorithms and can be applied to water bodies with a variety of turbidity levels and particle compositions. Future work will involve conducting studies on the generality of the POC/SPM estimation model and the robustness of the thresholds used to classify water bodies into different particle composition groups to further test or improve the accuracy and applicability of the new algorithm.

CRediT authorship contribution statement

Mailisu: . Dalin Jiang: Writing – review & editing, Investigation, Formal analysis, Data curation, Conceptualization. **Bunkei Matsushita:** Writing – review & editing, Visualization, Validation, Supervision, Resources, Project administration, Methodology, Investigation, Funding acquisition, Formal analysis, Data curation, Conceptualization.

Declaration of competing interest

The authors declare that they have no known competing financial interests or personal relationships that could have appeared to influence the work reported in this paper.

Acknowledgements

This research was supported in part by the Grants-in-Aid for Scientific Research of MEXT from Japan (No. 24 K01009).

Appendix A. Supplementary data

Supplementary data to this article can be found online at https://doi.org/10.1016/j.jag.2025.104909.

Data availability

All data are publicly available or available in the Supplementary Materials. If the manuscript is accepted for publication, the scripts used in the manuscript will be uploaded to GitHub.

References

Aas, E., 1996. Refractive index of phytoplankton derived from its metabolite composition. J. Plankton Res. 18, 2223–2249. https://doi.org/10.1093/plankt/18.12.2223.

Babin, M., Morel, A., Fournier-Sicre, V., Fell, F., Stramski, D., 2003. Light scattering properties of marine particles in coastal and open ocean waters as related to particle mass concentration. Limnol. Oceanogr. 48 (2), 843–859. https://doi.org/10.4319/lo.2003.48.2.0843.

Bailey, S.W., Werdell, P.J., 2006. A multi-sensor approach for the on-orbit validation of ocean color satellite data products. Remote Sens. Environ. 102 (1–2), 12–23. https://doi.org/10.1016/j.rse.2006.01.015.

Balasubramanian, S.V., Pahlevan, N., Smith, B., Binding, C., Schalles, J., Loisel, H., Gurlin, D., Greb, S., Alikas, K., Randla, M., Bunkei, M., Moses, W., Nguyễn, H., Lehmann, M.K., O'Donnell, D., Ondrusek, M., Han, T.-H., Fichot, C.G., Moore, T., Boss, E., 2020. Robust algorithm for estimating total suspended solids (TSS) in inland

and nearshore coastal waters. Remote Sens. Environ. 246, 111768. https://doi.org/10.1016/j.rse.2020.111768.
Beusen, A.H.W., Dekkers, A.L.M., Bouwman, A.F., Ludwig, W., Harrison, J., 2005. Estimation of global river transport of sediments and associated particulate C, N, and P. Glob. Biogeochem. Cycle 19, GB4S05. https://doi.org/10.1029/2005GB002453.
Brockmann, C., Doerffer, R., Peters, M., Stelzer, K., Embacher, S., Ruescas, A., 2016. Evolution of C2RCC Neural Network for Sentinel 2 and 3 for the Retrieval of Ocean Colour Products in Normal and Extreme Optically Complex Waters. Prague, Czech Republic, 9–13 May 2016. Available online: http://step.esa.int/docs/extra/EvolutionoftheC2RCC_LPS16.pdf (accessed on 25 June 202.
Doxaran, D., Ruddick, K., McKee, D., Gentili, B., Tailliez, D., Chami, M., Babin, M., 2009. Spectral variations of light scattering by marine particles in coastal waters, from the visible to the near infrared. Limnol. Oceanogr. 54 (4), 1257–1271. https://doi.org/10.4319/lo.2009.54.4.1257.
Eisma, D., 1993. Suspended matter in the aquatic environment. Springer, Berlin, Heidelberg. https://doi.org/10.1007/978-3-642-77722-6.
Gernez, P., Doxaran, D., Barillé, L., 2017. Shellfish aquaculture from space: potential of sentinel2 to monitor tide-driven changes in turbidity, chlorophyll concentration and oyster physiological response at the scale of an oyster farm. Front. Mar. Sci. 4, 137. https://doi.org/10.3389/fmars.2017.00137.
Han, B., Loisel, H., Vantrepotte, V., Mériaux, X., Bryère, P., Ouillon, S., Dessailly, D., Xing, Q., Zhu, J., 2016. Development of a semi-analytical algorithm for the retrieval of suspended particulate matter from remote sensing over clear to very turbid waters. Remote Sens. 8 (3), 211. https://doi.org/10.3390/rs8030211.
Harding, L.W., Magnuson, A., Mallonee, M.E., 2005. SeaWiFS retrievals of chlorophyll in Chesapeake Bay and the mid-Atlantic bight. Estuar. Coast. Shelf Sci. 62 (1–2), 75–94. https://doi.org/10.1016/j.ecss.2004.08.011.
Huynh, T.T., Kim, J., Lee, S.D., Fettweis, M., Bi, Q., Kim, S., Lee, S., Choi, Y.Y., Nguyen, H.S., Bui, T.V., Lee, B., J., 2024. Spatiotemporal dynamics of suspended particulate matter in water environments: a review. Water 16 (24), 3613. https://doi.org/10.3390/w16243613.
Ioccg, 2014. Phytoplankton functional types from space. In: Sathyendranath, S. (Ed.), Reports of the International Ocean-Colour Coordinating Group, No. 15. IOCCG, Dartmouth, Canada.
Jiang, D., Matsushita, B., Yang, W., 2020. A simple and effective method for removing residual reflected skylight in above-water remote sensing reflectance measurements. ISPRS-J. Photogramm. Remote Sens. 165, 16–27. https://doi.org/10.1016/j.isprsjprs.2020.05.003.
Jiang, D., Matsushita, B., Pahlevan, N., Gurlin, D., Lehmann, M.K., Fichot, C.G., Schalles, J., Loisel, H., Binding, C., Zhang, Y., Alikas, K., Kangro, K., Uusõue, M., Ondrusek, M., Greb, S., Moses, W.J., Lohrenz, S., O'Donnell, D., 2021. Remotely estimating total suspended solids concentration in clear to extremely turbid waters using a novel semi-analytical method. Remote Sens. Environ. 258, 112386. https://doi.org/10.1016/j.rse.2021.112386.
Jiang, D., Matsushita, B., Pahlevan, N., Gurlin, D., Fichot, C.G., Harringmeyer, J., Sent, G., Brito, A.C., Brotas, V., Werther, M., Mascarenhas, V., Blake, M., Hunter, P., Tyler, A., Spyrakos, E., 2023. Estimating the concentration of total suspended solids in inland and coastal waters from Sentinel-2 MSI: a semi-analytical approach. ISPRS-J. Photogramm. Remote Sens. 204, 362–377. https://doi.org/10.1016/j.isprsjprs.2023.09.020.
Lee, Z., Carder, K., Arnone, R., 2002. Deriving Inherent Optical Properties from Water Color: a Multiband Quasi-Analytical Algorithm for Optically Deep Waters. Appl. Opt. 41, 5755–5772.
Lehmann, M.K., Gurlin, D., Pahlevan, N., Alikas, K., Conroy, T., Anstee, J., Balasubramanian, S.V., Barbosa, C.C.F., Binding, C., Bracher, A., Bresciani, M., Burtner, A., Cao, Z., Dekker, A.G., Di Vittorio, C., Drayson, N., Errera, R.M., Fernandez, V., Ficek, D., Yue, L., 2023. GLORIA - a globally representative hyperspectral in situ dataset for optical sensing of water quality. Sci. Data 10 (1), 100. https://doi.org/10.1038/s41597-023-01973-y.
Liu, X., Sheng, Y., Liu, Q., Li, Z., 2024. Suspended particulate matter affects the distribution and migration of heavy metals in the Yellow River. Sci. Total Environ. 912, 169537. https://doi.org/10.1016/j.scitotenv.2023.169537.
Nechad, B., Ruddick, K.G., Park, Y., 2010. Calibration and validation of a generic multisensor algorithm for mapping of total suspended matter in turbid waters. Remote Sens. Environ. 114 (4), 854–866. https://doi.org/10.1016/j.rse.2009.11.022.
Neukermans, G., Loisel, H., Mériaux, X., Astoreca, R., McKee, D., 2012. In situ variability of mass-specific beam attenuation and backscattering of marine particles with respect to particle size, density, and composition. Limnol. Oceanogr. 57 (1), 124–144. https://doi.org/10.4319/lo.2012.57.1.0124.
Novoa, S., Doxaran, D., Ody, A., Vanhellemont, Q., Lafon, V., Lubac, B., Gernez, P., 2017. Atmospheric Corrections and Multi-Conditional Algorithm for Multi-Sensor Remote Sensing of Suspended Particulate Matter in Low-to-High Turbidity Levels Coastal Waters. Remote Sens. 9 (1), 61. https://doi.org/10.3390/rs9010061.
Reynolds, R.A., Stramski, D., Neukermans, G., 2016. Optical backscattering by particles in Arctic seawater and relationships to particle mass concentration, size distribution, and bulk composition. Limnol. Oceanogr. 61 (5), 1869–1890. https://doi.org/10.1002/lno.10341.
Shi, W., Wang, M., 2019. Characterization of suspended particle size distribution in global highly turbid waters from VIIRS measurements. J. Geophys. Res. 124 (6), 3796–3817. https://doi.org/10.1029/2018JC014793.
Siswanto, E., Tang, J., Yamaguchi, H., Ahn, Y.-H., Ishizaka, J., Yoo, S., Kim, S.-W., Kiyomoto, Y., Yamada, K., Chiang, C., Kawamura, H., 2011. Empirical ocean-color algorithms to retrieve chlorophyll-a, total suspended matter, and colored dissolved organic matter absorption coefficient in the Yellow and East China Seas. J. Oceanogr. 67 (5), 627–650. https://doi.org/10.1007/s10872-011-0062-z.
Stramski, D., Constantin, S., Reynolds, R.A., 2023. Adaptive optical algorithms with differentiation of water bodies based on varying composition of suspended particulate matter: a case study for estimating the particulate organic carbon concentration in the western Arctic seas. Remote Sens. Environ. 286, 113360. https://doi.org/10.1016/j.rse.2022.113360.
Szeligowska, M., Benkort, D., Przyborska, A., Moskalik, M., Moreno, B., Trudnowska, E., Błachowiak-Samołyk, K., 2024. Estimates of carbon sequestration potential in an expanding Arctic fjord (Hornsund, Svalbard) affected by dark plumes of glacial meltwater. Biogeosciences 21 (16), 3617–3639. https://doi.org/10.5194/bg-21-3617-2024.
Teng, W., Yu, Q., Stramski, D., Reynolds, R.A., Woodruff, J.D., Yellen, B., 2025. High spatial-resolution satellite mapping of suspended particulate matter in global coastal waters using particle composition-adaptive algorithms. Remote Sens. Environ. 323, 114745. https://doi.org/10.1016/j.rse.2025.114745.
Torregroza-Espinosa, A.C., Restrepo, J.C., Escobar, J., Brenner, M., Newton, A., 2020. Nutrient inputs and net ecosystem productivity in the mouth of the magdalena river. Colombia. Estuar. Coast. Shelf Sci. 243, 106899. https://doi.org/10.1016/j.ecss.2020.106899.
Wang, S., Li, X., Sun, D., He, X., Zhang, H., Zhao, W., He, Y., 2023. Satellite estimation of suspended particle types using a backscattering efficiency-based model in the marginal seas. Opt. Express 31 (2), 890. https://doi.org/10.1364/OE.476192.
Wang, S., Qiu, Z., Sun, D., Shen, X., Zhang, H., 2016. Light beam attenuation and backscattering properties of particles in the Bohai Sea and Yellow Sea with relation to biogeochemical properties. JGR Oceans 121 (6), 3955–3969. https://doi.org/10.1002/2016JC011727.
Woźniak, S.B., Darecki, M., Zabłocka, M., Burska, D., Dera, J., 2016. New simple statistical formulas for estimating surface concentrations of suspended particulate matter (SPM) and particulate organic carbon (POC) from remote-sensing reflectance in the southern Baltic Sea. Oceanologia 58 (3), 161–175. https://doi.org/10.1016/j.oceano.2016.03.002.
Woźniak, S. B., Stramski, D., Stramska, M., Reynolds, R. A., Wright, V. M., Miksic, E. Y., Cichocka, M., Cieplak, A. M., 2010. Optical variability of seawater in relation to particle concentration, composition, and size distribution in the nearshore marine environment at Imperial Beach, California. J. Geophys. Res.-Oceans 115(C8), 2009JC005554. https://doi.org/10.1029/2009JC005554.
Yang, W., Matsushita, B., Chen, J., Yoshimura, K., Fukushima, T., 2013. Retrieval of inherent optical properties for turbid inland waters from remote-sensing reflectance. IEEE Trans. Geosci. Remote Sensing 51 (6), 3761–3773. https://doi.org/10.1109/TGRS.2012.2220147.